Click Here for Full Article

Lateral entrapment of sediment in tidal estuaries: An idealized model study

K. M. H. Huijts,[1] H. M. Schuttelaars,[2] H. E. de Swart,[1] and A. Valle-Levinson[3]

Received 30 March 2006; revised 13 July 2006; accepted 10 August 2006; published 21 December 2006.

[1] Two physical mechanisms leading to lateral accumulation of sediment in tidally dominated estuaries are investigated, involving Coriolis forcing and lateral density gradients. An idealized model is used that consists of the three-dimensional shallow water equations and sediment mass balance. Conditions are assumed to be uniform in the along-estuary direction. A semidiurnal tidal discharge and tidally averaged density gradients are prescribed. The erosional sediment flux at the bed depends both on the bed shear stress and on the amount of sediment available in mud reaches for resuspension. The distribution of mud reaches over the bed is selected such that sediment transport is in morphodynamic equilibrium, that is, tidally averaged erosion and deposition of sediment at the bed balance. Analytical solutions are obtained by using perturbation analysis. Results suggest that in most estuaries lateral density gradients induce more sediment transport than Coriolis forcing. When frictional forces are small (Ekman number $E < 0.02$), the Coriolis mechanism dominates and accumulates sediment on the right bank (looking up-estuary in the Northern Hemisphere). On the other hand, when frictional forces are moderate to high ($E > 0.02$), the lateral density gradient mechanism dominates and entraps sediment in areas with fresher water. Results also show that the lateral sediment transport induced by the semidiurnal tidal flow is significant when frictional forces are small ($E \sim 0.02$). Model predictions are in good agreement with observations from the James River estuary.

Citation: Huijts, K. M. H., H. M. Schuttelaars, H. E. de Swart, and A. Valle-Levinson (2006), Lateral entrapment of sediment in tidal estuaries: An idealized model study, *J. Geophys. Res.*, *111*, C12016, doi:10.1029/2006JC003615.

1. Introduction

[2] Estuaries receive sediments from both fluvial and marine sources. Locally, large concentrations of suspended sediments are observed in many estuaries. These elevated suspended sediment concentrations appear in the vicinity of so called ''mud reaches,'' which are pools of easily erodible sediments on the bed [*Geyer*, 1993; *Sanford et al.*, 2001; *Woodruff et al.*, 2001; *North et al.*, 2004].

[3] Previous research on elevated suspended sediment concentrations has mainly focused on the along-estuary convergence of sediments. Many primarily observational studies [*Geyer et al.*, 2001; *Kappenberg and Grabemann*, 2001; *Lin and Kuo*, 2001; *North et al.*, 2004], report the presence of an estuarine turbidity maximum, which is a region containing the largest (cross-sectionally averaged) suspended sediment concentration [*Festa and Hansen*, 1978]. Relevant to the trapping of sediments in the along-estuary direction are river discharge [*Festa and Hansen*, 1976; *North et al.*, 2004], gravitational circulation [*Hansen and Rattray*, 1965; *Festa and Hansen*, 1978], tidal elevation and tidal velocity asymmetries [*Geyer*, 1993; *Jay and Musiak*, 1994; *Prandle*, 2004], wind [*North et al.*, 2004], bathymetry [*Festa and Hansen*, 1976], mud pools [*Uncles and Stephens*, 1993; *Sanford et al.*, 2001; *Jay and Musiak*, 1994; *Geyer et al.*, 1998] and flocculation [*Winterwerp*, 2002].

[4] In addition to along-estuary sediment trapping, most estuaries exhibit cross-channel variations in sediment concentration and bottom sediment type. For example, *Nichols* [1972] observed lateral sediment entrapment along the south channel shoulder of the James River. He also found that the grain size distribution varied widely from silty clay over the south channel shoulder to sand on the shoals. *Geyer et al.* [1998] and references therein reported accumulation of sediment along the shallow western bank of the Hudson estuary. Numerical simulations suggested this was partially caused by the convergence of near-bottom lateral currents driven by a lateral baroclinic pressure gradient and Coriolis accelerations.

[5] In this paper, we develop an idealized, process-oriented model to examine the effects of Coriolis forcing and lateral density gradient forcing on sediment entrapment in tidally dominated estuaries with arbitrary lateral bathymetry. Idealized models are appropriate for gaining fundamental physical understanding. Individual forcing mechanisms can be isolated, and their effects can be

[1]Institute for Marine and Atmospheric Research Utrecht, University of Utrecht, Utrecht, Netherlands.
[2]Delft Institute of Applied Mathematics, Delft University of Technology, Delft, Netherlands.
[3]Department of Civil and Coastal Engineering, University of Florida, Gainesville, Florida, USA.

Copyright 2006 by the American Geophysical Union.
0148-0227/06/2006JC003615$09.00

investigated in a systematic way. Moreover, solutions to idealized models are (semi)analytical, so that studying a problem under different parameter settings is straightforward.

[6] The model is two-dimensional in the lateral and vertical coordinate (analogous to the approach used by *Officer* [1976], *Kasai et al.* [2000], *Schramkowski and de Swart* [2002] and *Valle-Levinson et al.* [2003]), and is based on the shallow water equations, and the mass balance of sediments in suspension and at the bed, as described in Section 2. Motivated by *Friedrichs et al.* [1998], the distribution of easily erodible sediment in mud reaches at the bed is described by introducing a laterally varying erosion coefficient. Zero (large) values of the erosion coefficient represent no (a thick) mud reach at that location. More sediment is eroded from the bed if the erosion coefficient is larger or the bed shear stress increases. The erosion coefficient is selected such that lateral sediment transport is in morphodynamic equilibrium, that is, tidally averaged erosion of sediment balances deposition.

[7] A scaling and perturbation analysis is performed in section 3 to obtain a reduced and consistent set of model equations. Solving the equations analytically yields approximate solutions for the semidiurnal tidal flow, the mean (tidally averaged) flow and the mean suspended sediment concentration. Also, a semidiurnal correction to the mean sediment concentration is obtained, representing M_2-tidal variations in sediment concentration. In section 4, the effects of Coriolis deflection and lateral density gradients on the lateral entrapment of sediment in tidal estuaries are investigated. Also, the entrapment mechanisms are interpreted in terms the Ekman number. Model results are compared to observations in the James River estuary in section 5.

2. Model

[8] The model estuary is infinitely long with an arbitrary bottom profile of $z = -H(y)$ and a constant width B (see Figure 1). The maximum and minimum depth are denoted by H_{max} and H_{min}, respectively. The water motion is driven by an external M_2-tide with cross-sectional average velocity amplitude $U \sim 1$ m s^{-1} and angular frequency $\omega = 1.4 \times 10^{-4}$ s^{-1}. Moreover, along-estuary density gradients induce a mean flow with typical velocity $U_d \sim 0.1$ m s^{-1}. Lateral density gradients and Coriolis forcing cause lateral velocities with typical magnitude $V \sim 0.1$ m s^{-1}. For tidally dominated estuaries, typical river discharge velocities ($\sim$0.001–0.01 m s^{-1}) are small compared to density driven velocities, and are therefore neglected here.

[9] The sediment is assumed to consist of a single class of fine particles, which are transported as suspended load. The particles are assumed to be noncohesive. Sediment in suspension settles and deposits in the mud reach, which is a layer of erodible sediments on top of the nonerodible bottom at $z = -H(y)$. Conversely, this sediment is brought into suspension by bed shear stresses. We assume that the flow field is unaffected by the sediments. This requires that the erodible layer is thin compared to the water depth and that the sediment concentration ($\sim$10–100 mg L^{-1}) does not alter water density significantly.

[10] To focus on lateral processes, a local model description is used which describes a portion of the estuary of length L (Figure 1). The length $L \sim 1$ km is small compared to along-estuary length scales, such as tidal wavelength $\sim$400 km, tidal excursion length $\sim$10 km, and geometric length scales $\sim$5–40 km [*Friedrichs and Aubrey*, 1994]. The model description is uniform along the estuary, which means that the model is essentially two-dimensional with lateral and vertical coordinates. Because the length of the portion is much smaller than the tidal wavelength, variations in surface elevation are neglected, but barotropic pressure gradients are retained (rigid lid approximation [see, e.g., *Gill*, 1982]).

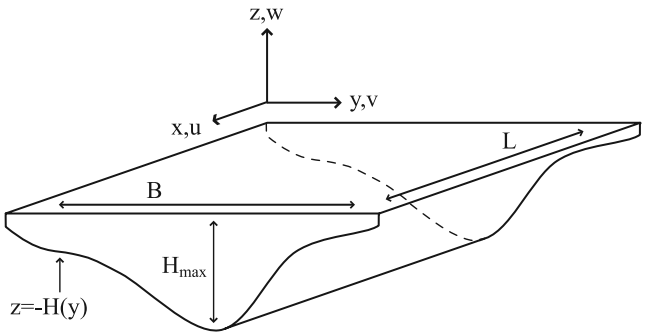

Figure 1. Sketch of the model geometry. A Cartesian coordinate system (x, y, z) is used, where the x axis points seaward, the y axis points to the left if looking seaward, and the z axis points upward. The bottom profile of the estuary is arbitrary in the lateral coordinate and extends uniformly in the along-estuary direction. The variables are introduced in the main text.

2.1. Hydrodynamics

[11] The governing equations for the hydrodynamics are the shallow water equations on the f-plane for along-estuary uniform conditions [*Schramkowski and de Swart*, 2002],

$$\frac{\partial u}{\partial t} + v\frac{\partial u}{\partial y} + w\frac{\partial u}{\partial z} - fv = \frac{g}{\rho_0}\frac{\partial \rho}{\partial x}z - g\frac{\partial \eta}{\partial x} + \frac{\partial}{\partial z}\left(A_z\frac{\partial u}{\partial z}\right), \quad (1a)$$

$$\frac{\partial v}{\partial t} + v\frac{\partial v}{\partial y} + w\frac{\partial v}{\partial z} + fu = \frac{g}{\rho_0}\frac{\partial \rho}{\partial y}z - g\frac{\partial \eta}{\partial y} + \frac{\partial}{\partial z}\left(A_z\frac{\partial v}{\partial z}\right), \quad (1b)$$

$$\frac{\partial v}{\partial y} + \frac{\partial w}{\partial z} = 0. \quad (1c)$$

Here u, v, and w denote the along-estuary, lateral and vertical velocity components (see Figure 1), t is time, $f \sim 10^{-4}$ s^{-1} is the Coriolis parameter, $g \sim 10$ m s^{-2} is gravitational acceleration, and $\rho_0 \sim 1020$ kg m^{-3} is a constant reference density. The along-estuary and lateral mean (tidally averaged) density gradients are prescribed and denoted by $\partial\rho/\partial x$ and $\partial\rho/\partial y$, respectively (both $\sim 10^{-3}$ kg m^{-4}). Focusing on partially to well-mixed estuaries, variations of both density gradients over depth are assumed to be negligible. The two components of the surface gradient, $\partial\eta/\partial x$ and $\partial\eta/\partial y$, are determined by the internal dynamics of the system (see conditions (3c) and (3d)). The vertical eddy

viscosity coefficient A_z is parameterized using the formulation of *Munk and Anderson* [1948],

$$A_z = A_0(1 + 10Ri)^{-1/2}. \quad (2)$$

Adopting the formulation of *Bowden et al.* [1959], the vertical eddy viscosity coefficient in the absence of stratification $A_0 = 2.5 \cdot 10^{-3} UH_0 \sim 10^{-3}$ m^2 s^{-1}, and $H_0 \sim 3$ m is half of the average depth. The Richardson number is taken as $Ri = g(\Delta\rho/\rho_0)\, H_0/U^2 \sim 0.5$, where $\Delta\rho$ is a typical density difference between bed and surface [*Dyer*, 1973]. Hence Ri and therefore A_z are constants.

[12] At the surface, we assume that the water motion is stress free and satisfies the kinematic boundary condition. Applying the rigid lid approximation yields

$$A_z \frac{\partial u}{\partial z} = A_z \frac{\partial v}{\partial z} = 0, \quad w = 0 \quad \text{at} \quad z = 0. \quad (3a)$$

At the bottom, we assume no slip and impermeability of the bottom,

$$u = v = w = 0 \quad \text{at} \quad z = -H. \quad (3b)$$

At the side boundaries, we assume that there is no lateral transport of water. As explained in auxiliary material Text S1[1], this implies that there is no lateral transport of water at any lateral location y,

$$\int_{-H}^{0} v\, dz = 0 \quad \text{for all } y. \quad (3c)$$

Hence the lateral water flux vanishes everywhere in the domain. Finally, a semidiurnal tidal discharge with amplitude $Q = AU$ and frequency ω is imposed by

$$\frac{1}{A}\int_0^B \int_{-H}^{0} u\, dz\, dy = U\cos(\omega t), \quad (3d)$$

where A is the area of the cross section and B is the width of the estuary. Note that conditions (3c) and (3d) ensure mass conservation (see auxiliary material Text S1). By imposing these two conditions, the along-estuary and lateral surface gradients $\partial\eta/\partial x$ and $\partial\eta/\partial y$ are determined.

2.2. Sediment Dynamics

[13] The sediment dynamics of the model are governed by the sediment mass balance equation for along-estuary uniform conditions,

$$\frac{\partial c}{\partial t} + \frac{\partial}{\partial y}\left(vc - K_y\frac{\partial c}{\partial y}\right) + \frac{\partial}{\partial z}\left((w - w_s)c - K_z\frac{\partial c}{\partial z}\right) = 0. \quad (4)$$

Here c denotes the suspended sediment concentration, w_s is the settling velocity ($\sim$1 mm s^{-1}) and K_y and K_z are constant lateral and vertical eddy diffusivity coefficients. *Fischer et al.*'s [1979, section 7.3] work has been used to select $K_y = 5$ m^2 s^{-1}, and K_z is parameterized following *Munk and Anderson* [1948]

$$K_z = K_0(1 + 3.33Ri)^{-3/2}, \quad (5)$$

where $K_0 = A_0$ is the vertical eddy diffusivity coefficient in the absence of stratification.

[14] We require that the lateral sediment transport vanishes at the side boundaries (in agreement with no lateral transport of water at the side boundaries, see equation (102) in auxiliary material Text S1),

$$\int_{-H}^{0}\left(vc - K_y\frac{\partial c}{\partial y}\right)dz = 0 \quad \text{at} \quad y = 0,\ B. \quad (6a)$$

At the surface, the diffusive and settling sediment flux balance,

$$w_s c + K_z\frac{\partial c}{\partial z} = 0 \quad \text{at} \quad z = 0. \quad (6b)$$

Furthermore, the flux of sediment normal to the bed induced by erosion, E_s, is modeled as

$$E_s \equiv -K_y\frac{\partial c}{\partial y}n_y - K_z\frac{\partial c}{\partial z}n_z = w_s c_* \quad \text{at} \quad z = -H, \quad (6c)$$

where $\mathbf{n} = (0, n_y, n_z)$ is the upward unit vector that is normal to the bottom and c_* is a reference concentration. The reference concentration is determined by the density of the sediment ρ_s, a (dimensionless) bed shear stress, $\tau_b/(\rho_0 g' d_s)$, and a (dimensionless) laterally varying erosion coefficient $a(y)$, modeling the amount of sediment at the bed available for resuspension,

$$c_*(y,t) = \rho_s\frac{|\boldsymbol{\tau}_b(y,t)|}{\rho_0 g' d_s}a(y). \quad (7)$$

Here d_s denotes the grain size of the sediment, $g' = g(\rho_s - \rho_0)/\rho_0$ is the reduced gravity, and

$$\boldsymbol{\tau}_b = \boldsymbol{\rho}_0 A_z\frac{\partial \mathbf{u}}{\partial z} \quad \text{at} \quad z = -H, \quad (8)$$

where $\mathbf{u} \equiv (u, v, w)$. The bed shear stress is assumed to be much larger than the critical bed shear stress for erosion of sediments. For the sediments under consideration (coarse silt), typical values are $\rho_s = 2650$ kg m^{-3}, $g' = 16$ m s^{-2} and $d_s = 20$ μm. The erosion coefficient $a(y) \sim 10^{-5}$ models the lateral distribution of easily erodible sediment in mud reaches in a simplified way: A larger value of the erosion coefficient indicates a thicker mud reach. Hence, when more sediment is available for erosion or the bed shear stress is larger, more sediment is eroded into the water column (by equation (7)).

[15] At this point, the vertical and temporal structure of the suspended sediment concentration is fully determined. In the next section, the lateral structure of the sediment concentration is determined as well by deriving an equation for the erosion coefficient $a(y)$.

2.3. Mud Reaches at Morphodynamic Equilibrium

[16] A typical timescale over which the easily erodible sediment redistributes after the forcing has changed (for example increased river discharge during spring) is much smaller ($\sim$days) than the typical timescale over which the

[1] Auxiliary materials are available in the HTML. doi:10.1029/2006JC003615.

Table 1. Default Parameter Values Representative for a Typical Tidal Estuary

Quantity	Symbol	Value
Maximum water depth	H_{max}	12 m
Minimum water depth	H_{min}	1 m
Average half depth	H_0	3 m
Width of transect	B	5 km
Average tidal velocity amplitude	U	0.4 m s^{-1}
Angular tidal frequency	ω	1.4×10^{-4} s^{-1}
Coriolis parameter	f	$8.8 \times 10^{-5} s^{-1}$
Gravitational acceleration	g	10 m s^{-2}
Reference density	ρ_0	1020 kg m^{-3}
Along-estuary density gradient	$\partial\rho/\partial x$	0.5×10^{-3} kg m^{-4}
Lateral density gradient	$\partial\rho/\partial y$	1×10^{-3} kg m^{-4}
Bed to surface density difference	$\Delta\rho$	2 kg m^{-3}
Fall velocity	w_s	0.3 mm s^{-1}
Reference erosion coefficient	a_*	4×10^{-6}

forcing remains in the new situation (∼weeks−months). Therefore we consider a system in which there is no mean evolution of the bed, $\langle \partial z_b/\partial t \rangle$, where z_b is the position of the bed and the angular brackets $\langle \cdot \rangle$ denote a tidal average or mean. This is referred to as a system in morphodynamic equilibrium.

[17] An equation for the time evolution of the bed [*Van Rijn*, 1993] is given by

$$\rho_s(1-p)\frac{\partial z_b}{\partial t} = D - E_s, \tag{9}$$

where ρ_s and p are the density and porosity of the sediment, and D is the depositional sediment flux normal to the bottom defined by

$$D \equiv w_s c\, n_z \quad \text{at} \quad z = -H. \tag{10}$$

No mean evolution of the bed requires a mean balance between deposition and erosion, $\langle D \rangle - \langle E_s \rangle = 0$ (equation (9)).

[18] A relation between mean deposition minus erosion and mean lateral sediment transport can be obtained by integrating sediment mass balance equation (4) over depth, and exchanging integration and differentiation using Leibniz rule. Also, boundary conditions (3a), (3b) and (6b) are used, as well as definitions (6c) and (10) for E_s and D, and the result is averaged over a tidal period.

[19] Using the relation between erosion minus deposition and transport derived in the previous paragraph as well as (6a) shows that a mean balance between deposition and erosion requires a mean balance of the advective and diffusive sediment transport in the lateral direction,

$$\int_{-H}^{0} \left(\langle vc \rangle - K_y \left\langle \frac{\partial c}{\partial y} \right\rangle \right) dz = 0 \quad \text{for all } y. \tag{11}$$

This condition is referred to as the morphodynamic equilibrium condition.

[20] By (6c) and (7), the sediment concentration varies linearly with the erosion coefficient. Hence the morphodynamic equilibrium condition (11) can be rewritten into a first-order linear differential equation for the erosion coefficient $a(y)$,

$$I_1 \frac{da}{dy} + I_2 a = 0. \tag{12}$$

Here I_1 and I_2 are known integrals given by

$$I_1 = \int_{-H}^{0} -K_y \langle c/a \rangle dz,$$
$$I_2 = \int_{-H}^{0} \left(\langle v(c/a) \rangle - K_y \frac{\partial \langle c/a \rangle}{\partial y} \right) dz. \tag{13}$$

To determine the integration constant which arises in solving equation (12), an additional condition is required,

$$\frac{1}{B}\int_0^B a(y)dy = a_*. \tag{14}$$

Hence the shape of the erosion coefficient determined by (12) ensures a morphodynamic equilibrium. The average amount of sediment available in mud reaches for resuspension is modeled by imposing a reference value $a_* \sim 10^{-5}$ by condition (14). Hence a_* is prescribed such that the desired order of magnitude of sediment concentration values are obtained.

3. Perturbation Analysis and Solutions

[21] In this section, perturbations solutions to the system of equations presented in section 2 are obtained which are applicable to a typical tidal estuary. The relative order of magnitude of the terms in the model are found by performing a scaling analysis, which is described in auxiliary material Text S2, and using the default parameter values given in Table 1 (see section 4 for a description of the default estuary). A small parameter $\varepsilon \equiv V/U \sim 0.1$ is introduced comparing a typical scale for the lateral velocity $V \sim 0.1$ m s^{-1} to the average tidal velocity amplitude U. Besides, eight nondimensional parameters characterizing the system are identified, and their magnitude relative to the small parameter ε are estimated. These parameters and their order of magnitude in a typical tidally dominated estuary are given in Table 2. Solutions to the scaled system of equations are constructed as perturbation series in powers of the small parameter up to order ε,

$$\widetilde{\Psi} = \widetilde{\Psi}_0 + \varepsilon \widetilde{\Psi}_1, \tag{15}$$

with Ψ being any of the variables u, v, w, $\partial\eta/\partial x$, $\partial\eta/\partial y$ or c, a tilde ($\widetilde{\ }$) denoting a dimensionless variable, and the

Table 2. Order of Magnitude of Nondimensional Parameters As Assumed in the Scaling Analysis in Auxiliary Material Text S2, and Their Actual Value Using the Parameter Values Given in Table 1

Nondimensional Parameter	Assumption	Value
$\varepsilon \equiv V/U$	$\mathcal{O}(0.1)$	0.1
f/ω	$\mathcal{O}(1)$	0.6
$A_z/(\omega H_0^2)$	$\mathcal{O}(1)$	1
$K_z/(\omega H_0^2)$	$\mathcal{O}(1)$	0.7
$w_s/(\omega H_0)$	$\mathcal{O}(1)$	0.7
$\partial\rho/\partial y/(\partial\rho/\partial x)$	$\mathcal{O}(1)$	2
$K_y/(VB)$	$\mathcal{O}(0.1)$	0.03
U_d/U	$\mathcal{O}(0.1)$	0.3
$V/(\omega B)$	$\mathcal{O}(0.01)$	0.06

subscript denoting the order of the component. By substituting this expansion in the scaled system of equations and collecting terms with equal powers of ε, a dominant order system of equations (ε^0 terms) and a higher-order system of equations (ε^1 terms) are obtained. The resulting reduced systems of equations and morphodynamic equilibrium condition are given in sections 3.1, 3.2 and 3.3, respectively. The dominant and higher-order system of equations are solved analytically. See auxiliary material Text S2 for the solution methods and analytical solutions.

3.1. Dominant Order System of Equations

[22] The $\mathcal{O}(\varepsilon^0)$ equations for the flow field are given by

$$\frac{\partial u_0}{\partial t} = -g\frac{\partial \eta_0}{\partial x} + A_z\frac{\partial^2 u_0}{\partial z^2}, \tag{16a}$$

$$fu_0 = -g\frac{\partial \eta_0}{\partial y} + A_z\frac{\partial^2 v_0}{\partial z^2}, \tag{16b}$$

$$\frac{\partial v_0}{\partial y} + \frac{\partial w_0}{\partial z} = 0. \tag{16c}$$

The flow component at dominant order satisfies no slip and no normal flow at the bottom, stress free surface, no normal flow through the surface, no lateral transport of water, and is forced by the external M_2-tide analogous to (3). For convenience, a second subscript is introduced to denote at what tidal harmonic a particular term oscillates. Hence the tidal flow at dominant order can be specified by $\mathbf{u}_{02}$. The resulting along-estuary flow is the consequence of a balance between local accelerations, surface gradient forcing and is damped by turbulent friction. Note that this scaling indicates that the lateral flow is forced at the semidiurnal frequency by the Coriolis forcing, but not by the local acceleration. The lateral surface gradient responds to the forcing, and frictional effects are present again.

[23] The suspended sediment concentration at dominant order is determined by the balance between local inertia, vertical settling and diffusive effects,

$$\frac{\partial c_0}{\partial t} - w_s\frac{\partial c_0}{\partial z} - K_z\frac{\partial^2 c_0}{\partial z^2} = 0. \tag{17}$$

Boundary conditions at dominant order are no sediment flux through the surface analogous to (6b), and the erosional sediment flux at the bottom prescribed by

$$-K_z\frac{\partial c_0}{\partial z} = w_s\rho_s\frac{|\boldsymbol{\tau}_b|_0}{\rho_0 g' d_s}a \quad \text{at} \quad z = -H. \tag{18}$$

Here the zeroth order component of the absolute value of the bed shear stress $|\boldsymbol{\tau}_b|_0$ is related to the tidal flow by

$$|\boldsymbol{\tau}_b|_0 = \rho_0 A_z\left|\frac{\partial \mathbf{u}_{02}}{\partial z}\right| \quad \text{at} \quad z = -H. \tag{19}$$

Hence the sediment concentration at dominant order results from tidal resuspension of sediment during ebb and flood, and deposition of sediment during the slack tides in between.

[24] Harmonic analysis of (19) shows that the dominant order sediment concentration can be written as a Fourier series which contains a mean term and the even overtides of the semidiurnal tide, such that

$$c_0 = c_{00} + c_{04} + \dots . \tag{20}$$

3.2. Higher-Order System of Equations

[25] The $\mathcal{O}(\varepsilon^1)$ equations for the flow field are governed by

$$\frac{\partial u_1}{\partial t} - fv_0 = \frac{g}{\rho_0}\frac{\partial \rho}{\partial x}z - g\frac{\partial \eta_1}{\partial x} + A_z\frac{\partial^2 u_1}{\partial z^2}, \tag{21a}$$

$$\frac{\partial v_0}{\partial t} + fu_1 = \frac{g}{\rho_0}\frac{\partial \rho}{\partial y}z - g\frac{\partial \eta_1}{\partial y} + A_z\frac{\partial^2 v_1}{\partial z^2}, \tag{21b}$$

$$0 = \frac{\partial v_1}{\partial y} + \frac{\partial w_1}{\partial z}, \tag{21c}$$

subject to no slip and no normal flow at the bottom, stress free surface and no normal flow through the surface and no lateral transport of water, similar to (3a)–(3c). Also, the cross-sectionally averaged mean flow vanishes analogous to (3d), but the right hand side is zero. Hence the higher-order flow component experiences a mean forcing by horizontal density gradients and is also forced at the M_2 frequency by the zeroth-order tidal flow. Thus the solution of the first-order velocity field can be written as $\mathbf{u}_1 = \mathbf{u}_{10} + \mathbf{u}_{12}$.

[26] The equation and boundary conditions for the suspended sediment concentration at first order are equivalent to those at zeroth order, with the first-order component of the absolute value of the bed shear stress,

$$|\boldsymbol{\tau}_b|_1 = \rho_0 A_z\left(\frac{\partial \mathbf{u}_0}{\partial z}\cdot\frac{\partial \mathbf{u}_1}{\partial z}\right)\Big/\left|\frac{\partial \mathbf{u}_0}{\partial z}\right| \quad \text{at} \quad z = -H. \tag{22}$$

Hence the first-order sediment concentration results from the interaction of the dominant order tidal flow ($\mathbf{u}_0$) and the higher-order flow ($\mathbf{u}_1$).

[27] Harmonic analysis of (22) shows that the first-order sediment concentration consists of all tidal constituents, i.e.,

$$c_1 = c_{10} + c_{12} + \dots . \tag{23}$$

Here the residual component and the even overtides of M_2 result from the semidiurnal part of the higher-order flow, $\mathbf{u}_{12}$, and include the nonlinear part of the bed shear stress caused by the semidiurnal tidal flow. On the other hand, the M_2 constituent and its odd overtides are caused by the residual part of the higher-order flow, $\mathbf{u}_{10}$, and thus emerge from tidal asymmetries in the flow.

3.3. Morphodynamic Equilibrium Condition

[28] The morphodynamic equilibrium condition up to $\mathcal{O}(\varepsilon)$ is given by

$$\int_{-H}^{0}\left(\langle v_0 c_0\rangle + \langle v_1 c_0\rangle + \langle v_0 c_1\rangle - K_y\left\langle\frac{\partial c_0}{\partial y}\right\rangle\right)dz = 0 \text{ for all } y. \tag{24}$$

Substituting $v_0 = v_{02}$, $v_1 = v_{10} + v_{12}$, (20) and (23) for the dominant and higher-order flow and sediment concentration yields

$$T_{M_0} + T_{M_2} + T_{diff} \equiv \int_{-H}^{0} \left(v_{10} c_{00} + \langle v_{02} c_{12} \rangle - K_y \frac{\partial c_{00}}{\partial y} \right) dz = 0. \tag{25}$$

Hence the system is in morphodynamic equilibrium if the mean lateral sediment transport induced by the mean flow, T_{M_0}, by the semidiurnal flow u_{02}, T_{M_2}, and by diffusion, T_{diff}, balance.

[29] Note that in estuarine studies, mean transport induced by tidal flow is often ignored or modeled as turbulent diffusion, whereas this work suggests that mean transport induced by tidal flow can be quite important. This result is supported by for example *Jay and Smith* [1990], who showed the importance of accounting for tide-induced salt fluxes in partially mixed estuaries. Crucial for its importance is the phase difference between the lateral tidal velocity and the semidiurnal sediment concentration. The more these two quantities are in phase, the larger their contribution to the mean lateral sediment transport.

4. Lateral Sediment Entrapment Mechanisms

[30] In this section, the model is used to identify two physical mechanisms leading to lateral sediment entrapment in weakly nonlinear, tidally dominated estuaries. The mechanisms are related to Coriolis deflection of along-estuary flow (section 4.1), and lateral density gradients (section 4.2), respectively. In section 4.3, the relative importance of the two mechanisms is related to the Ekman number.

[31] The default parameter values used in this section are given in Table 1, and represent a typical tidal estuary such as the lower James River Estuary in Virginia, USA [*Valle-Levinson et al.*, 2000; *Nichols*, 1972]. The model estuary consists of a main channel in the middle, that is flanked by relatively narrow shoals (depths of 12 and 1 meter, respectively). The width is 5 kilometers and the model bathymetry is symmetric about the mid-axis,

$$H = H_{max} \exp\left[-\left(y - \frac{1}{2}B \right)^2 \Big/ l^2 \right], \tag{26}$$

where l is $0.3B$. A semidiurnal external tidal constituent is imposed with an average velocity amplitude of 0.4 m s^{-1}. The Coriolis parameter is 8.8×10^{-5} s^{-1}, which means that the estuary is in the Northern Hemisphere and flow is deflected to the right by Coriolis forcing. The mean (tidally averaged) along-estuary and lateral density gradient is 0.5 and 1 kg m^{-3} per kilometer, respectively. Hence water density increases linearly from the river toward the sea, and from the left shore toward the right shore (looking up-estuary). The bed to surface density difference is taken 2 kg m^{-3}, which yields a bulk Richardson number of 0.4 (see section 2.1) and $A_z = 0.001$ m^2 s^{-1} and $K_z = 0.0009$ m^2 s^{-1} (see equations (2) and (5)). The sediment under consideration is silty clay with a settling velocity of 0.3 mm s^{-1} [*Dyer*, 1986]. The reference erosion coefficient a_* is chosen such that the maximum of the resulting mean sediment concentration is approximately 20 mg L^{-1}. The order of magnitude of the nondimensional parameters corresponding to the default parameter values in Table 1 are as assumed in the scaling analysis (Table 2), except that $V/(\omega B)$ is an order of magnitude larger than assumed, as discussed in auxiliary material Text S2.

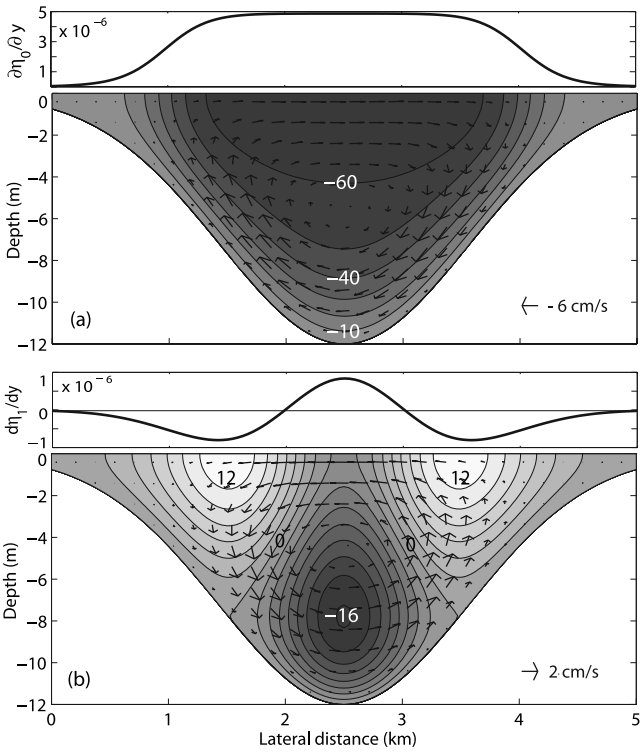

Figure 2. Results for the Coriolis mechanism showing the along-estuary (contours) and transverse (arrows) components of the (a) semidiurnal tidal flow at maximum flood and (b) mean (tidally averaged) flow. Parameter values are as given in Table 1, but $\partial\rho/\partial y = 0$. Orientation of this and subsequent figures is looking into the estuary. Negative values (dark gray) denote inflow, whereas positive values (light gray) denote outflow. Contour interval is 10 cm s^{-1} for Figure 2a and 2 cm s^{-1} for Figure 2b, and largest arrow in the lower part of the water column represents lateral flow of -6 cm s^{-1} in Figure 2a and 2 cm s^{-1} in Figure 2b. Note the difference in scale between the lateral and vertical axis. The semidiurnal component at maximum flood (Figure 2a), and the mean component (Figure 2b) of the lateral surface gradient are added as well.

4.1. Coriolis Mechanism

[32] In many estuaries, an external semidiurnal tide and a mean (tidally averaged) along-estuary density gradient induce along-estuary flows (a tidal flow and an estuarine gravitational circulation, respectively). In this section, we investigate how Coriolis deflection of these flows effects the mean lateral entrapment of sediment. The effects of a lateral density gradient on sediment entrapment are excluded here by taking $\partial\rho/\partial y = 0$ (remaining values are as displayed in Table 1).

[33] Figure 2a shows the tidal flow field and the lateral surface gradient at maximum flood. The figure shows that

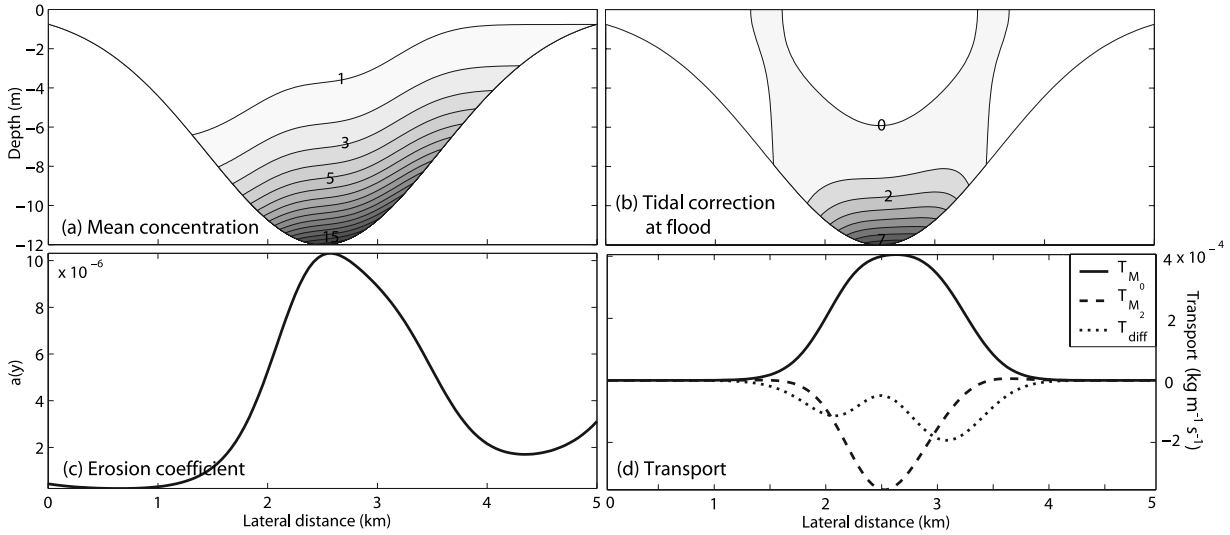

Figure 3. Results for the Coriolis mechanism showing (a) the tidally averaged suspended sediment concentration c_{00}, (b) a semidiurnal correction to the mean sediment concentration, c_{12}, at flood, (c) the erosion coefficient, and (d) mean lateral sediment transport induced by the mean flow (solid line), tidal flow (dashed line) and diffusion (dotted line). Contour interval in Figures 3a and 3b is 1 mg L^{-1}. In Figure 3c, a larger value of the erosion coefficient indicates a thicker mud reach at that location.

the along-estuary tidal flow increases from bed to surface with maximum values of 65 cm s^{-1} above the deep channel. The transverse tidal flow shows a circulation pattern with velocities up to 6 cm s^{-1}: At maximum flood, a positive lateral flow is induced by Coriolis deflection of the along-estuary tidal flow [see *Lerczak and Geyer*, 2004]. Superimposed on that, there is a negative barotropic flow induced by the lateral surface slope which ensures mass conservation. The circulation pattern persists during slack tide and reverses during the ebb (not shown).

[34] Figure 2b shows the mean (tidally averaged) flow and lateral surface slope. The along-estuary component can be considered as part of the estuarine gravitational circulation [see, e.g., *Van de Kreeke and Zimmerman*, 1990] with mean landward flow over the deep channel and mean seaward flow over the shallow sides. Maximum velocity is -16 cm s^{-1}. A circulation cell with velocities up to 2 cm s^{-1} is present in the transverse plane. This secondary circulation pattern results from Coriolis deflection of the along-estuary mean flow (negative lateral velocities in the outflow regions over the sides and positive lateral velocities in the inflow region over the deep channel) and lateral surface gradient forcing, which ensures mass conservation.

[35] Sediment distributions and transport in morphodynamic equilibrium are displayed in Figure 3. The dominant component of the mean (tidally averaged) distribution of suspended sediment, c_{00} (see equations (15) and (20)), is displayed in Figure 3a, showing that sediments are trapped over the right bank (looking up-estuary). Figure 3b shows a small semidiurnal correction, c_{12} (see equations (15) and (23)) to this mean sediment concentration, displayed at maximum flood. Hence Figures 3a and 3b show that sediment concentrations during flood (ebb) increase (decrease) with at most 7 mg/L compared to mean concentrations of up to 15 mg/L. The erosion coefficient is displayed in Figure 3c, showing the presence of a mud reach on the right side ($a(y)$ large). Figure 3d shows that the mean flow transport T_{M_0} toward the right is balanced by the tidal flow transport T_{M_2} and the diffusive transport T_{diff} toward the left. Note that the lateral distribution of the erosion coefficient was selected by requiring no mean lateral sediment transport (see morphodynamic equilibrium condition (12)). T_{M_0} is positive, as the mean suspended sediment concentration decreases with distance from the bed (Figure 3a), such that the majority of the sediment transport is induced by the lateral flow in the lower part of water column, which is toward the right (Figure 2a). T_{M_2} is negative, as semidiurnal concentrations at maximum flood are positive (Figure 3b) and lateral near-bed flow is leftward (Figure 2). This situation persists at slack tide after the flood (not shown). During ebb and slack tide after the ebb, transport is still leftward, as both flow and semidiurnal concentrations are of opposite sign (not shown).

4.2. Lateral Density Gradient Mechanism

[36] In many estuaries, mean (tidally averaged) density gradients are observed in the lateral direction. In this section, we investigate how these lateral density gradients effect the mean lateral entrapment of sediment. The effects of lateral density gradients are isolated from the effects of Coriolis deflection of along-estuary flows (section 4.1) by taking $f = 0$. Two characteristic distributions of density over the lateral direction are considered. First, water is saltier at a side, which is prescribed by a constant lateral density gradient (default value given in Table 1). For a symmetric bed profile and in the absence of Coriolis forcing, such a gradient could result from inflow of fresh water from a tributary at a side. Second, water is saltier in the channel, or the mean density is distributed parabolically over the lateral direction. Such a distribution is imposed by a linear lateral density gradient with average magnitude being the default value given in Table 1. Without Coriolis forcing or asymmetries in the bed profile, such a gradient could result from

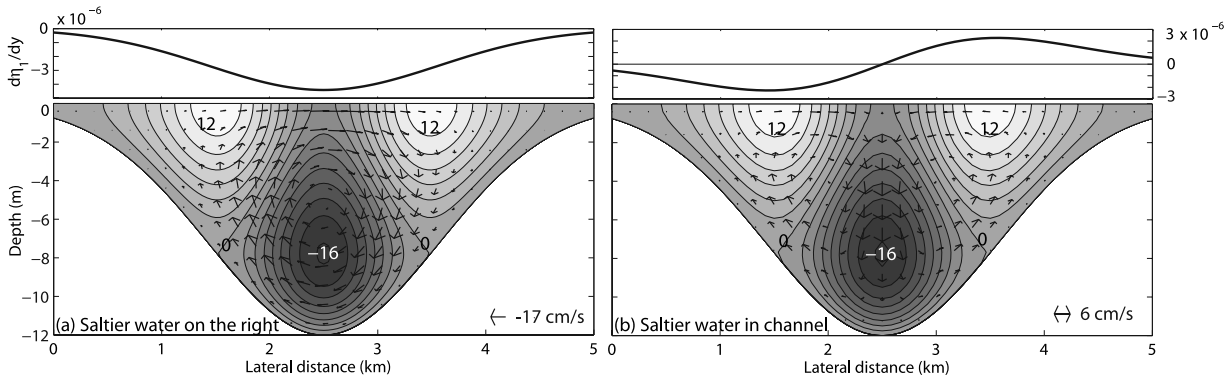

Figure 4. Mean flow and lateral surface gradient induced by a (a) constant and (b) linear lateral density gradient. Largest arrow in lower part of the water column represents a lateral velocity of -17 cm s^{-1} in Figure 4a and ± 6 cm s^{-1} in Figure 4b.

advection of salt by the mean gravitational circulation: Tidally averaged, saltier water is advected up-estuary over the deep channel, whereas fresher water is advected down-estuary over the shoals (see contours in Figure 2b). Alternatively, saltier water being over channel could result from differential advection of salt because the tidal wave propagates faster over deeper areas and stratification varies over a tidal cycle as described by *Lerczak and Geyer* [2004]. The remaining parameter values are as given in Table 1.

[37] Figure 4 shows the mean flow and mean lateral surface gradient for (Figure 4a) a constant and (Figure 4b) a linearly increasing density gradient. The along-estuary mean flow (contours in Figure 4) and semidiurnal tidal flow (not shown) are identical to Figure 4 because the same along-estuary forcing (tides and along-estuary density gradient) are applied. There is no transverse semidiurnal flow, as Coriolis forcing is neglected here. The arrows in Figure 4 represent the mean cross-sectional flow. If water is denser at the right, a single circulation cell emerges across the estuary with velocities up to 17 cm s^{-1} (Figure 4a). If water is saltier in the channel than over the shoals (Figure 4b), two counter-rotating circulation cells are generated across the estuary. Maximum velocity of this two-cell circulation pattern is about 6 cm s^{-1} with convergent surface flow and divergent bottom flow.

[38] The transverse circulation cells in Figure 4 are induced by a mechanism similar to the vertical gravitational circulation in the along-estuary direction: Averaged over depth, the baroclinic pressure gradient force induced by the lateral density gradient is balanced by a barotropic pressure gradient force induced by the lateral surface slope (the lateral surface slope arises to ensure mass conservation). In the lower part of the water column, the baroclinic forcing dominates over the barotropic forcing, resulting in a mean flow from the saltier toward the fresher water. In the upper part of the water column the barotropic forcing dominates such that mean flow is in the opposite direction.

[39] The transverse flow induced by a lateral density gradient is fundamentally different from the transverse flow induced by Coriolis deflection of along-estuary flow. The lateral density gradient directly forces a transverse circulation, which implies that transverse velocities (Figure 4) are relatively strong compared to the indirectly induced transverse velocities by the Coriolis forcing (Figure 2).

[40] Figures 5 and 6 display how a constant and linear density gradient affect the sediment distributions and transport. Sediments are entrapped in areas with fresher water (Figures 5a and 6a and Figures 5c and 6c). The direction of the mean lateral flow near the bed determines the direction of the transport by the mean flow (see near-bed arrows in Figure 4) and T_{M_0} in Figures 5d and 6d). Since there is no lateral semidiurnal flow, the semidiurnal tidal concentration shown in Panels b do not affect the mean lateral transport of sediment ($T_{M_2} = 0$ in Figures 5d and 6d). The diffusive transport T_{diff} balances T_{M_0}.

4.3. Trapping Mechanisms in Terms of Ekman Number

[41] The previous subsections showed that the Coriolis mechanism competes against (or reinforces) the lateral density gradient mechanism if they are both present: Coriolis deflection of along-estuary flow entraps sediments over the right bank (looking up-estuary in the Northern Hemisphere), whereas lateral density gradients trap sediments in relatively fresh water. Moreover, it was shown that both the mean flow (by means of both mechanisms) and the semidiurnal tidal flow (by means of the Coriolis mechanism only) contributed to the mean lateral sediment transport. In this section, the relative importance of the two mechanisms is explored in terms of the Ekman number. First, we focus on the sediment transport induced by the mean flow T_{M_0}. The importance of the sediment transport induced by the semidiurnal tidal flow T_{M_2} is discussed later in this subsection.

[42] By separating T_{M_0} into a contribution caused by the Coriolis mechanism

$$T_{M_0,f} \equiv \int_{-H}^{0} v_{10,f}\, c_{00}\, dz,$$

and a contribution caused by the lateral density gradient mechanism

$$T_{M_0,\partial\rho/\partial y} \equiv \int_{-H}^{0} v_{10,\partial\rho/\partial y}\, c_{00}\, dz,$$

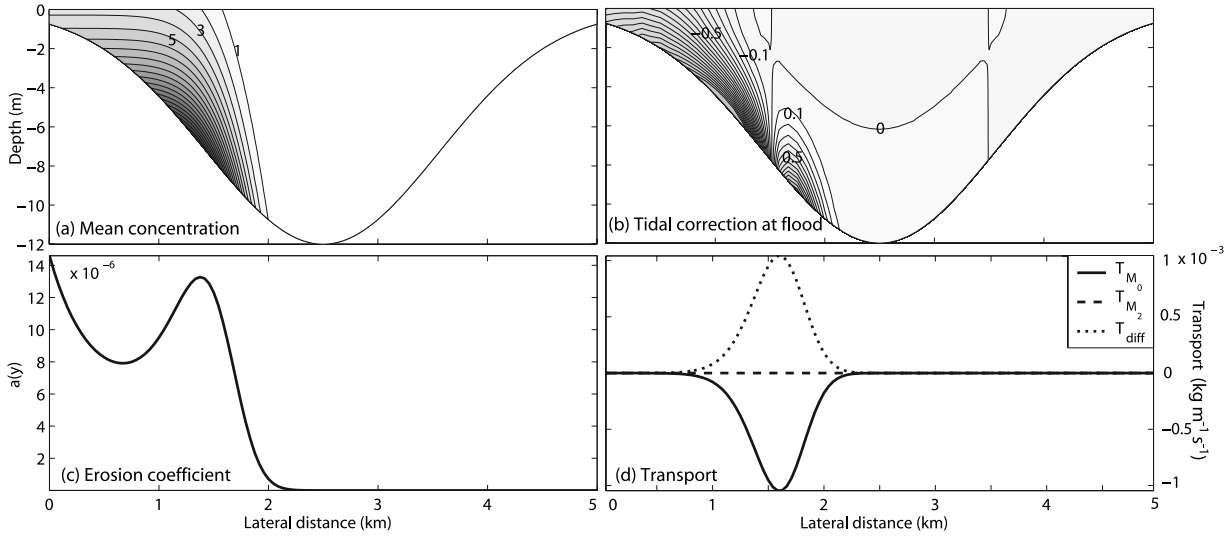

Figure 5. Effects of a constant lateral density gradient representing saltier water on the right on (a) the tidally averaged suspended sediment concentration, (b) a semidiurnal correction to the mean sediment concentration at flood, (c) the erosion coefficient, and (d) the mean lateral sediment transport. Contour interval is 1 mg L^{-1} in Figure 5a and 0.1 mg L^{-1} in Figure 5b.

the relative importance of both mechanisms can be studied. Here $v_{10,f}$ is the mean lateral flow induced by the Coriolis mechanism and $v_{10,\partial\rho/\partial y}$ is the mean lateral flow induced by the lateral density gradient mechanism. Both of them can be obtained from the solution for the total mean lateral flow (see auxiliary material Text S2). The ratio of these two velocities is a good approximation for the relative importance of the sediment transport contributions (which can be seen from the solution for the mean sediment concentration in auxiliary material Text S2 and the expressions for the transport contributions given above). Using these solutions, the approximation for the relative importance of the sediment transport contributions can be expressed in terms of the Ekman number and the ratio of the horizontal density gradients, i.e.,

$$\frac{T_{M_0,\partial\rho/\partial y}}{T_{M_0,f}} \approx \frac{v_{10,\partial\rho/\partial y}}{v_{10,f}} \sim E\frac{\partial\rho/\partial y}{\partial\rho/\partial x}, \tag{27}$$

where $E = A_z/(f\,H_{\max}^2)$ is the vertical Ekman number. Hence, according to the model, the expression on the right hand side is crucial in determining whether sediments accumulate over the right or left bank. Moreover, data from

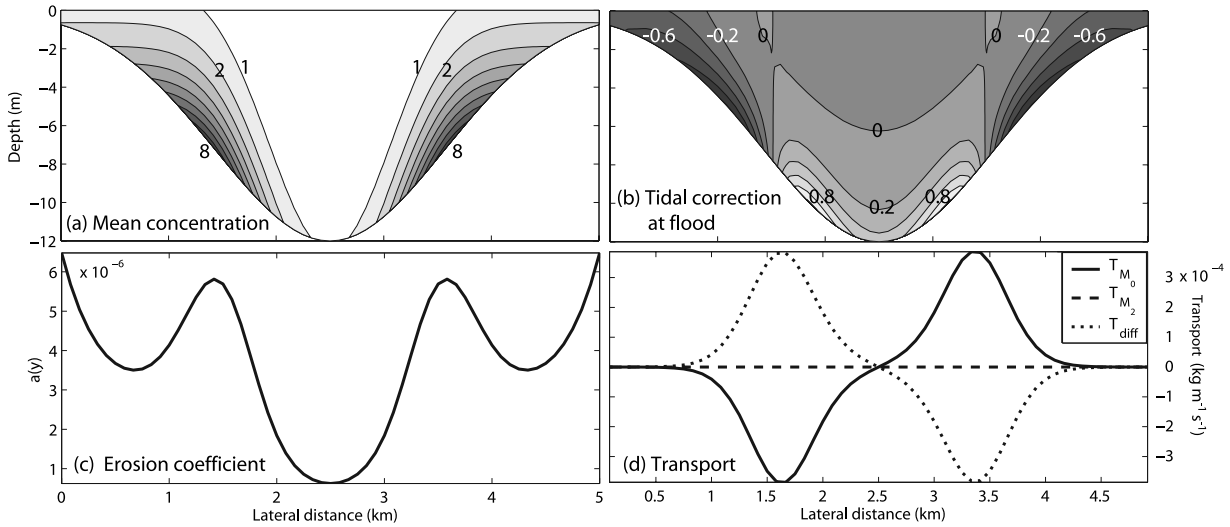

Figure 6. Effects of a linear lateral density gradient representing saltier water in the channel on (a) the mean suspended sediment concentration, (b) a semidiurnal correction to the mean concentration at flood, (c) the erosion coefficient, and (d) the mean lateral sediment transport. Contour interval is 1 mg L^{-1} in Figure 6a and 0.2 mg L^{-1} in Figure 6b.

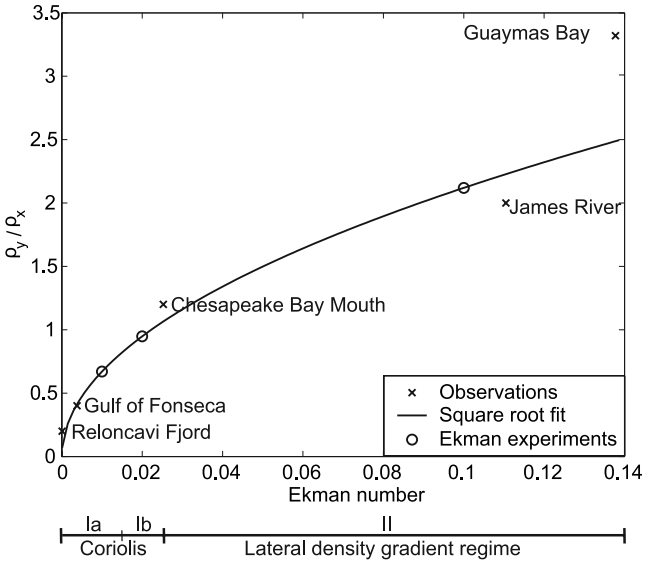

Figure 7. Dependence of the ratio of the horizontal density gradients on the Ekman number. The crosses represent data from five different estuaries (Reloncavi Fjord is stratified and deep, the Gulf of Fonseca is weakly stratified but deep, the Chesapeake Bay mouth is partially stratified and moderately deep, James River is partially mixed and shallow, and Guaymas Bay is a vertically homogeneous, shallow coastal lagoon; see *Valle-Levinson and Bosley* [2003], *Valle-Levinson and Lwiza* [1997], *Valle-Levinson et al.* [2000, 2001], and A. Valle-Levinson et al., Spatial structure of hydrography and flow in a Chilean Fjord, Estuario Reloncav, submitted to *Estuaries*, 2006). The solid line is fitted to the observations and suggests a square root dependence of the ratio of the density gradients on the Ekman number. The circles represent the combination of values selected for the experiments in which the Ekman number was varied. The Coriolis and the lateral density gradient regime (see main text) are indicated by I and II, respectively.

five estuaries ranging from low to highly frictional suggest that the estimate of the transport ratio (right-hand side of (27)) is determined by the Ekman number only, since the ratio of the horizontal density gradients seems to depend on the Ekman number by a square root dependence (Figure 7).

[43] The following experiment was performed. Adopting the square root dependence suggested by the data in Figure 7, parameter settings yielding Ekman numbers 0.01, 0.02 and 0.1 (circles in Figure 7) representing Ekman number regimes Ia, Ib and II (see Figure 7). Fixed values for the Coriolis parameter, maximum water depth and along-estuary density gradient were used (default values given in Table 1, except for $\partial\rho/\partial x = 1 \times 10^{-4}$ kg m^{-4}), the vertical eddy viscosity coefficient A_z was chosen to obtain the selected Ekman numbers, and the lateral density gradient was determined from the square root dependence. The vertical eddy diffusivity coefficient was estimated by simply taking $K_z = A_z$.

[44] Results for the mean suspended sediment concentration and mean lateral sediment transport for the three selected Ekman numbers are shown in Figure 8. Figures 8a–8c show that the position of the trapped sediments indeed changes from right to left with increasing friction. The associated increase in the eddy diffusivity coefficient is reflected in an increase of the *e*-folding length scale of the suspended sediment concentration. Figures 8d and 8f show that the sediment is mainly transported laterally by the mean flow (T_{M_0}) and by diffusive processes (T_{diff}) in regime Ia and II, whereas the contribution by the tidal flow T_{M_2} is small. However, in regime Ib (Panel (e)) the transport T_{M_2} is dominant. This is caused by a relatively low contribution of the transport by the mean flow T_{M_0} (compared to regime Ia and II), as $T_{M_0,\partial\rho/\partial y}$ and $T_{M_0,f}$ cancel each other to a large extent. Therefore the Coriolis regime (I) can be divided into two subregimes: In regime Ia, the sediment transport by the flow is mainly caused by Coriolis deflection of a mean flow ($T_{M_0,f}$), whereas in regime Ib, the transport by the tidal flow T_{M_2} is important as well. Note that the values for the Ekman number indicating transition from one (sub)regime to another as indicated in Figure 7 would change if the suggested relation between the ratio of the horizontal density gradients and the Ekman number would not be adopted or would be changed (as can be seen from (27)).

5. Comparison to Observations

[45] In this section, we illustrate how the model can be applied to a real estuary to gain insight in the effects of a particular forcing on the flow field and to identify the mechanisms causing lateral entrapment of sediment in that estuary. Also, we show how model results compare to observations.

[46] We consider a cross section of the James River, Virginia, where detailed observations of flow and acoustic backscatter (a proxy for sediment concentration) profiles were obtained in October 1996 during two spring tidal cycles (see *Valle-Levinson et al.* [2000] for details). The default parameters values (see Table 1) are used, as they apply to this transect. In particular, the lateral density gradient observed in the James River cross section is characterized by a constant value representing saltier water at the right. Note that for the observed asymmetric transect, this is equivalent to saltier water being in the channel, as the right shoal is very small. Hence the mechanisms suggested in section 4.2 inducing the two typical lateral distributions of density in the absence of Coriolis forcing may apply to the James. Another possible mechanism causing the observed lateral density gradient is Coriolis forcing [*Valle-Levinson et al.*, 2000]. As the default parameter values apply to the James River transect, Table 2 shows that the model assumptions are also reasonably satisfied for this transect. The bathymetry observed in the James River cross section as shown in Figure 9 is used. Hence comparing the results presented in this section to the appropriate results shown in the previous section yields insight in effects on the flow and sediment distributions caused by asymmetries in the bed profile.

[47] Model results reproduce the essential features of the observed semidiurnal tidal current amplitude (Figure 9). Largest amplitudes appear in the channel and the isopaches follow the bathymetry in response to frictional effects. The mean flow obtained analytically also resembles the observations closely (Figure 10). Mean inflow is restricted to the

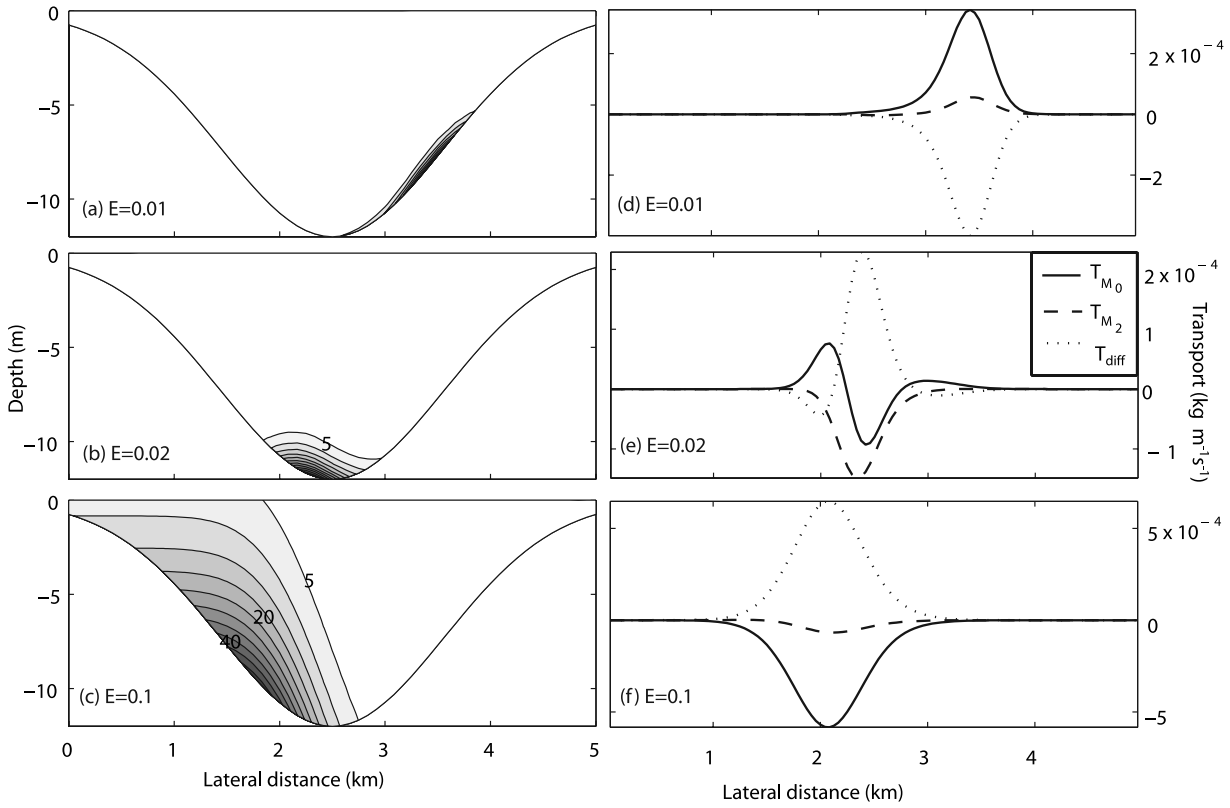

Figure 8. Dependence of (a–c) the mean suspended sediment concentration and (d–f) the mean lateral transport of sediments on the Ekman number. Contour interval in Figures 8a–8c is 5 mg L^{-1}. The line style in Figures 8d–8f indicates transport by the mean flow (dashed line), tidal flow (dotted line) and diffusion (solid line).

channel and occupies the entire water column, whereas mean outflows appear over a depth of ~6 m. The mean lateral flows feature near-surface flow from left to right (looking into the estuary in Figure 10) and near-bottom flow toward the left bank. The lateral distribution of the mean flow suggests a moderate Ekman number [*Valle-Levinson et al.*, 2003], indicating the importance of frictional effects in producing such flows (E = 0.1 in the James River). Indeed, the mean lateral circulation predicted by the model is caused by the lateral density gradient mechanism, which was suggested in the previous section to be dominant in a moderate to highly frictional regime.

[48] In order to compare suspended sediment concentrations obtained from the model with observations in the James River, acoustic backscatter data were used to obtain a proxy for the sediment concentration. The conversion from mean acoustic backscatter data BK to mean suspended sediment concentration C was effected with the relationship C = 0.03 mg L^{-1} exp(0.097 BK), derived from a calibration for this estuary [*Battisto and Friedrichs*, 2003]. Although this relationship may not exactly apply to the observations obtained in 1996, the functionality of the relationship has remained consistent in different parts of Chesapeake Bay [*Friedrichs et al.*, 2003]. Therefore the distribution of C displayed in Figure 11 may not be quantitatively correct but should qualitatively represent appropriate C distributions across the estuary. The pattern thus obtained compares very well with that predicted by the model and is also in

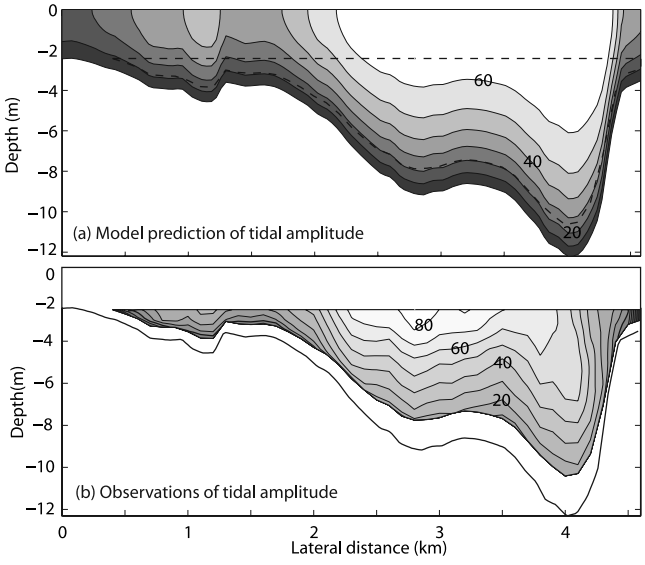

Figure 9. Comparison of (a) model predictions and (b) observations of the amplitude of the along-estuary semidiurnal tidal flow for a transect in the James River estuary. Contour interval is 10 cm s^{-1}. No observations are available in the upper 2 meters and in the lowest 15 percent of the water column. The dashed line in Figure 9a and subsequent figures indicates the area of observations.

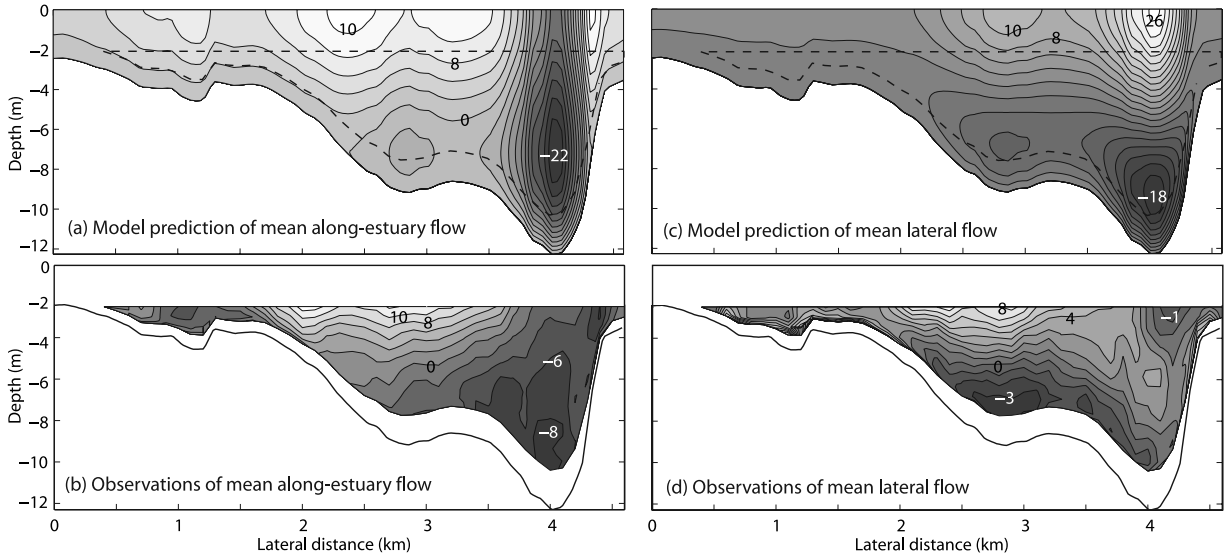

Figure 10. Comparison of (a, c) model predictions and (b, c) observations of the (a, b) along-estuary and (c, d) lateral mean flow for a transect in the James River estuary. Contour interval is 2 cm s^{-1} in Figures 10a–10c and 1 cm s^{-1} in Figure 10d.

agreement with observations reported by *Nichols* [1972]. Hence the model suggests that the mud reach found along the left bank of the James River (E = 0.1) result from the lateral density gradient mechanism, which is in agreement with the analysis for the moderate to high Ekman number regime as presented in section 4.3.

6. Discussion

[49] The results presented in section 4 showed that both Coriolis deflection of the along-estuary flow (mechanism 1) and lateral density gradients (mechanism 2) cause lateral entrapment of sediment. Coriolis deflection of the estuarine gravitational circulation (mechanism 1a) resulted in a mean transverse circulation cell. The cell transports the mean sediment concentration laterally into the direction of the near-bed flow. Similarly, Coriolis deflection of the along-estuary semidiurnal tidal flow (mechanism 1b) induced a semidiurnal circulation in the cross section. Because of tidal asymmetries in the sediment concentration (represented by a semidiurnal correction to the mean sediment concentration), the time-oscillating transverse circulation cell induces mean lateral sediment transport as well. Its direction and magnitude depended on the direction of the near-bed semidiurnal flow and its phase difference with the semidiurnal contribution to the concentration. The amount of sediment transported laterally by Coriolis deflection of the along-estuary tidal flow was comparable to the amount transported by Coriolis deflection of the mean along-estuary flow. A laterally varying erosion coefficient (modeling the distribution of mud reaches over the bed) was selected such that the mean lateral sediment transport by diffusion and advection balanced and a morphodynamic equilibrium situation was obtained. Coriolis deflection of along-estuary flow resulted in equilibrium mud pools and elevated sediment concentrations over the right bank (looking up-estuary in the Northern Hemisphere).

[50] A constant (linear) lateral density gradient (mechanism 2) caused a single (two counter-rotating) mean transverse circulation pattern(s). Mud pools and elevated sediment concentrations were found in the cross-sectional region(s) with relatively fresh water.

[51] The two transport mechanisms reinforce each other or compete, depending on the lateral distribution of the density and the Hemisphere in which the estuary is situated. However, the lateral density gradient mechanism is expected to be more important than the Coriolis mechanism

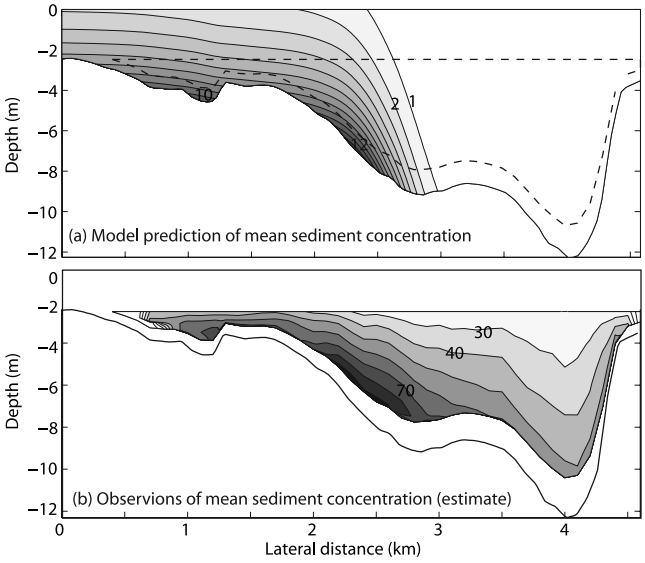

Figure 11. Comparison of (a) model predictions and (b) observations (approximation based on backscatter data) of the mean suspended sediment concentration for a transect in the James River estuary. The contour interval is 1 mg L^{-1} in Figure 11a and 10 mg L^{-1} in Figure 11b.

in many tidal estuaries. This is because a lateral density gradient directly induces lateral flow (and hence lateral sediment transport), whereas Coriolis deflection of along-estuary flow induces lateral flow only indirectly. Explaining the relative importance of the two mechanism in terms of the Ekman number (see section 4.3) also supports the dominance of the lateral density gradient mechanism, as many estuaries are in the lateral density gradient regime (Regime II in Figure 7 with Ekman number $E > 0.02$). Note that, although Coriolis deflection of the along-estuary flow seems to play a minor role in many tidal estuaries, the along-estuary flow is crucial for lateral transport of sediment, as it creates a substantial part of the bed shear stress that resuspends the bed sediments.

[52] Even though the model seems to represent the essential features of the flow and sediment deposition in the James, some physical mechanisms are not represented yet. Among these are nonlinear advective terms, curvature of riverbanks, sediment resuspension by wind waves, critical bed shear stress, wind stress, and temporal and spatial variations in stratification and mixing conditions (caused by, e.g., tidal straining).

7. Conclusions

[53] In this paper, the effects of individual physical forcing (by tides and horizontal density gradients) on flow and lateral sediment entrapment in a cross section of a tidally dominated, weakly nonlinear estuary have been studied in a systematic way. A two-dimensional idealized model was obtained using a scaling and perturbation analysis. Resuspension of sediment at the bed depends both on the bed shear stress and on the amount of sediment available in mud reaches for resuspension. The distribution of mud reaches over the bed is selected such that sediment transport is in morphodynamic equilibrium, that is, tidally averaged lateral transport of sediment by advection by the flow and by diffusion balance.

[54] Lateral sediment entrapment mechanisms related to Coriolis deflection of along-estuary flows and lateral density gradients were identified. On the basis of model results and data, it was suggested that which forcing dominates the entrapment of sediment across an estuary (and the generation of mean lateral flow) is characterized in terms of the Ekman number E. The Coriolis mechanisms is dominant for low Ekman numbers ($E < 0.02$), resulting in mean accumulation of sediment on the right slope of the channel (looking into a Northern Hemisphere estuary). On the other hand, the lateral density gradient mechanism dominates for Ekman numbers larger than 0.02, resulting in sediment entrapment in the cross-sectional regions with relatively fresh water. Results also showed that for very low Ekman numbers ($E < 0.01$), the dominant sediment transport is induced by Coriolis deflection of the estuarine gravitational circulation, whereas for low Ekman numbers in the range $0.01 < E < 0.02$ the dominant transport is induced by Coriolis deflection of the tidal flow. It is likely that in most systems the lateral density gradient mechanism dominates. Therefore sediment entrapment tends to occur over the regions with relatively fresh water.

[55] A comparison of model results to observations in the James River estuary ($E = 0.11$) showed that the model predictions are qualitatively in good agreement with data. Moreover, it showed that the lateral density gradient mechanism indeed dominates the Coriolis mechanism in the James River transect and causes accumulation of sediments on the left side (looking into the estuary), as observed.

[56] **Acknowledgments.** We are grateful to Stefan Talke for his help in improving the manuscript.

References

Battisto, G. M., and C. T. Friedrichs (2003), Monitoring suspended sediment plume formed during dredging using ADCP, OBS, and bottle samples, in *Coastal Sediments 2003: Crossing Disciplinary Boundaries* (CD-ROM), edited by R. A. Davis, A. H. Sallenger Jr., and P. Howd, World Sci., Hackensack, N. J.

Bowden, K. F., L. A. Fairbairn, and P. Hughes (1959), The distribution of shearing stresses in a tidal current, *Geophys. J. R. Astron. Soc.*, *2*, 288–305.

Dyer, K. R. (1973), *Estuaries: A Physical Introduction*, 2nd ed., John Wiley, Hoboken, N. J.

Dyer, K. R. (1986), *Coastal and Estuarine Sediment Dynamics*, John Wiley, Hoboken, N. J.

Festa, J. F., and D. V. Hansen (1976), A two-dimensional numerical model of estuarine circulation: The effects of altering depth and river discharge, *Estuarine Coastal Mar. Sci.*, *4*, 309–323.

Festa, J. F., and D. V. Hansen (1978), Turbidity maxima in partially mixed estuaries: A two-dimensional numerical model, *Estuarine Coastal Mar. Sci.*, *7*, 347–359.

Fischer, H. B., E. J. List, R. Y. C. Koh, J. Imberger, and N. H. Brooks (1979), *Mixing in Inland and Coastal Waters*, Elsevier, New York.

Friedrichs, C. T., and E. G. Aubrey (1994), Tidal propagation in strongly convergent channels, *J. Geophys. Res.*, *99*(C2), 3321–3336.

Friedrichs, C. T., B. D. Armbrust, and H. E. de Swart (1998), Hydrodynamics and equilibrium sediment dynamics of shallow, funnel-shaped tidal estuaries, in *Physics of Estuaries and Coastal Seas*, edited by J. Dronkers and M. B. A. M. Scheffers, pp. 315–327, A. A. Balkema, Brookfield, Vt.

Friedrichs, C. T., L. H. Brasseur, M. E. Scully, and S. E. Suttles (2003), Use of backscatter from acoustic Doppler current profiler to infer eddy diffusivity of sediment and bottom stress, in *Coastal Sediments 2003: Crossing Disciplinary Boundaries* (CD-ROM), edited by R. A. Davis, A. H. Sallenger Jr., and P. Howd, World Sci., Hackensack, N. J.

Geyer, W. R. (1993), The importance of suppression of turbulence by stratification on the estuarine turbidity maximum, *Estuaries*, *16*, 113–125.

Geyer, W. R., R. P. Signell, and G. C. Kineke (1998), Lateral trapping of sediment in a partially mixed estuary, in *Physics of Estuaries and Coastal Seas*, edited by J. Dronkers and M. B. A. M. Scheffers, pp. 115–124, A. A. Balkema, Brookfield, Vt.

Geyer, W. R., J. D. Woodruff, and P. Traykovski (2001), Sediment transport and trapping in the Hudson river estuary, *Estuaries*, *24*, 670–679.

Gill, A. E. (1982), *Atmosphere-Ocean Dynamics*, *Int. Geophys. Ser.*, vol. 30, Elsevier, New York.

Hansen, D. V., and M. Rattray Jr. (1965), Gravitational circulation in straits and estuaries, *J. Mar. Res.*, *23*, 104–122.

Jay, D. A., and J. D. Musiak (1994), Particle trapping in estuarine tidal flows, *J. Geophys. Res.*, *99*(C10), 445–461.

Jay, D. A., and J. D. Smith (1990), Residual circulation in shallow estuaries: 2. Weakly stratified and partially mixed, narrow estuaries, *J. Geophys. Res.*, *95*(C1), 733–748.

Kappenberg, J., and I. Grabemann (2001), Variability of the mixing zones and estuarine turbidity maxima in the Elbe and Weser estuaries, *Estuaries*, *24*, 699–706.

Kasai, A., A. E. Hill, T. Fujiwara, and J. H. Simpson (2000), Effect of the Earth's rotation on the circulation in regions of freshwater influence, *J. Geophys. Res.*, *105*(C), 19,961–19,969.

Lerczak, J. A., and W. R. Geyer (2004), Modeling the lateral circulation in straight, stratified estuaries, *J. Phys. Oceanogr.*, *34*, 1410–1428.

Lin, J., and A. Y. Kuo (2001), Secondary turbidity maximum in a partially mixed microtidal estuary, *Estuaries*, *24*, 707–720.

Munk, W. H., and E. R. Anderson (1948), Notes on a theory of the thermocline, *J. Mar. Res.*, *7*, 276–295.

Nichols, M. M. (1972), Sediments of the James River estuary, Virginia, *Mem. Geol. Soc, Am.*, *133*, 169–210.

North, E. W., S. Y. Chao, L. P. Sanford, and R. R. Hood (2004), The influence of wind and river pulses on an estuarine turbidity maximum: Numerical studies and field observations in Chesapeake Bay, *Estuaries*, *27*, 132–146.

Officer, C. B. (1976), *Physical Oceanography of Estuaries (and Associated Coastal Waters)*, John Wiley, Hoboken, N. J.

Prandle, D. (2004), Saline intrusion in partially mixed estuaries, *Estuarine Coastal Shelf Sci.*, *59*, 385–397.

Sanford, L. P., S. E. Suttles, and J. P. Halka (2001), Reconsidering the physics of the Chesapeake Bay estuarine turbidity maximum, *Estuaries*, *24*, 655–669.

Schramkowski, G. P., and H. E. de Swart (2002), Morphodynamic equilibrium in straight tidal channels: Combined effects of Coriolis force and external overtides, *J. Geophys. Res.*, *107*(C12), 3227, doi:10.1029/2000JC000693.

Uncles, R. J., and J. A. Stephens (1993), The freshwater-saltwater interface and its relationship to the turbidity maximum in the Tamar estuary, United Kingdom, *Estuaries*, *16*, 126–141.

Valle-Levinson, A., and K. T. Bosley (2003), Reversing circulation patterns in a tropical estuary, *J. Geophys. Res.*, *108*(C10), 3331, doi:10.1029/2003JC001786.

Valle-Levinson, A., and K. M. M. Lwiza (1997), Bathymetric influences on the lower Chesapeake Bay hydrography, *J. Mar. Syst.*, *12*, 221–236.

Valle-Levinson, A., K. C. Wong, and K. M. M. Lwiza (2000), Fortnightly variability in the transverse dynamics of a coastal plain estuary, *J. Geophys. Res.*, *105*(C2), 3413–3424.

Valle-Levinson, A., J. A. Delgado, and L. P. Atkinson (2001), Reversing water exchange patterns at the entrance to a semiarid coastal lagoon, *Estuarine Coastal Shelf Sci.*, *53*, 825–838.

Valle-Levinson, A., C. Reyes, and R. Sanay (2003), Effects of bathymetry, friction, and rotation on estuary-ocean exchange, *J. Phys. Oceanogr.*, *33*, 2375–2393.

Van de Kreeke, J., and J. T. F. Zimmerman (1990), Gravitational circulation in well- and partially-mixed estuaries, in *The Sea*, vol. 9a, edited by B. Le Mehaute and D. M. Hanes pp. 495–521, John Wiley, Hoboken, N. J.

Van Rijn, L. C. (1993), *Principles of Sediment Transport in Rivers, Estuaries and Coastal Seas*, Aqua, Amsterdam.

Winterwerp, J. C. (2002), On the flocculation and settling velocity of estuarine mud, *Coastal Shelf Res.*, *22*, 1339–1360.

Woodruff, J. D., W. R. Geyer, C. K. Sommerfield, and N. W. Driscoll (2001), Seasonal variation of sediment deposition in the Hudson River estuary, *Mar. Geol.*, *179*, 105–119.

H. E. de Swart and K. M. H. Huijts, Institute for Marine and Atmospheric Research Utrecht, University of Utrecht, Princetonplein 5, NL-3584 CC Utrecht, Netherlands. (k.m.h.huijts@phys.uu.nl)

H. M. Schuttelaars, Delft Institute of Applied Mathematics, Delft University of Technology, Mekelweg 4, NL-2600 GA, Delft, Netherlands.

A. Valle-Levinson, Department of Civil and Coastal Engineering, University of Florida, 365 Weil Hall, P.O. Box 116580, Gainesville, FL 32611, USA.